Korean J. Chem. Eng., 35(6), 1354-1364 (2018)
DOI: 10.1007/s11814-018-0029-5

pISSN: 0256-1115
eISSN: 1975-7220

Organosilicon resin-based carbon/ceramic polygranular composites with improved oxidation resistance

Krystian Sokolowski*, Aneta Fraczek-Szczypta*, Janusz Tomala, and Stanislaw Blazewicz*,†**

*Department of Biomaterials and Composites, Faculty of Materials Science and Ceramics, AGH - University of Science and Technology, Al. Mickiewicza 30, 30-059 Cracow, Poland
**SGL Carbon Polska S.A., ul. Piastowska 29, 47-400 Raciborz, Poland
(*Received 23 October 2017 • accepted 9 February 2018*)

Abstract−We examined the thermo-mechanical properties of carbon materials modified with silicon oxycarbide (Si-O-C) and silicon carbide (Si-C). These compounds were obtained by the impregnation of carbon components with a silicon-containing polymer resin. Graphite and anthracite powders were used as carbon components, and poly[methyl(phenyl)siloxane] resin (P) was used as the ceramic precursor. Carbon/polymer compositions (C/P) were subjected to two-stage annealing, first to 1,000 °C and next to 2,000 °C in an inert atmosphere, leading to the formation of C/Si-O-C and C/Si-C composite samples, respectively. The materials were then examined under conditions of isothermal oxidation to determine their oxidation resistance and the mechanical properties before and after oxidation tests. The structure of the samples before and after oxidation was studied. C/Si-C composites, despite their high porosity, proved to have enhanced resistance to oxidation at 600 °C, although they had lower mechanical properties in comparison to C/Si-O-C samples.

Keywords: Polysiloxane Resin, Carbon Materials, Silicon Oxycarbide, Silicon Carbide, Oxidation Resistance

INTRODUCTION

Carbon-based materials are of particular interest due to their appealing physical and chemical properties [1]. They stand out among other groups of materials due to their low density and excellent thermo-mechanical properties and are stable up 2,300 °C in an inert atmosphere [2,3]. However, in the presence of gaseous oxidants they begin to degrade at around 300 °C, due to their high susceptibility to oxygen. To reduce this negative impact, improved oxidation resistance and relevant protection of the physical and mechanical properties is required [1,3].

There are many methods of protecting the attractive properties of carbon-based materials, based on the modification of the material's structure or microstructure, or the introduction of an extra material which eliminates the source of oxidation in given circumstances [1,4,5]. However, the effectiveness of these methods depends on the temperature of application [3,4]. Between 400 °C and 600 °C, oxygen reacts with active carbon atoms, which are present mainly in its porous structure. Such an effect can be partially reduced either by graphitization or the introduction of inhibitors in the form of glass-forming substances, i.e., Si, P, and B elements, their oxides, or other compounds [6-8]. Above 600 °C, the oxidation process is determined by microstructural defects which facilitate the transportation of oxygen [1,3,4]. At 800 °C and higher, the diffusing oxygen reacts with the whole surface [4,9].

The concept of protection relies on the formation of a non-permeable layer to separate the gas-carbon reaction substrates [5,10, 11]. As well as higher application functionality in regard to the surface, material selection criteria for such tight layers also include their physical and chemical compatibility (coefficient of thermal expansion, adhesion) [5,9,11]. Ceramic compounds, such as the carbides, nitrides, and borides of highly-fusible elements, e.g., silicon or hafnium, meet these criteria [11-14]. All of these materials remain stable at clearly defined temperature ranges. Compounds such as SiC and Si_3N_4 are often used due to their high thermal stability at elevated temperatures in various applications [13,15-17]. However, currently available technologies, including conventional sintering, advanced chemical reactions (CVD), and liquid (sol-gel) phase reactions, often require the use of expensive substrates, have a high energy consumption, and do not always meet the standards in regard to the form of the final product [18,19]. Therefore, an alternative solution might be the introduction of polysiloxane resins, which, when heat treated in an inert atmosphere, convert to ceramic phases in the form of silicon oxycarbide (Si-O-C, at around 1,000 °C) and silicon carbide (Si-C, at around 2,000 °C) [20-22].

Our aim was to analyze the thermo-mechanical properties of carbon-based materials modified with ceramic residues, which were obtained through the heat treatment of polymers containing silicon in their chain structure.

EXPERIMENTAL

1. Materials

The carbon compounds used were synthetic graphite (denoted G) and gas-calcined anthracite (denoted A) with grain fractions of up to 250 μm.

†To whom correspondence should be addressed.
E-mail: blazew@agh.edu.pl

Table 1. Preceramic polymers characteristics

Catalogue reference number	Labelling	Solubility	Non-volatile components (%)	Ceramic residue (%)	C/Si	O/Si
L4102 polymethylfenylsiloxanes	P	Acetone	Min. 78	74,79	3,11	1,17

Table 2. Coal tar pitch characteristics

Properties	Range	Value	Based on
Softening point - Mettler [°C]	101-105	103,3	DIN 51920/84
Coking values - Alcan (%)	Min. 54	54,0	DIN 51905/81
QI amount (%)	6-9	6,3	DIN 51921/85
TI amount (%)	Min. 24	24,0	DIN 51906/81
Ash (%)	Max. 0,5	0,130	DIN 51922/83
Sulphur (%)	Max. 0,6	0,450	LECO

As a precursor of the ceramic component, poly[methyl(phenyl)siloxane] L4102 resin (denoted resin P) (Czech Lučební závody a.s. Kolín company) was used. The structure of this polymer consists of a high molecular chain with alternating Si-O elements, and a side chain with silicon-attached methyl and phenyl groups. The base characteristics of resin P are shown in Table 1 [18].

Reference samples were manufactured from conventional coal tar pitch (CTP), which is utilized in synthetic carbon and graphite technology as a binder and carbon precursor, and is available on the market. The base properties of CTP are presented in Table 2.

2. Sample Preparation

To investigate the influence of the preparation method, samples were prepared by two procedures shown in Fig. 1. According to the first procedure (denoted S), powdered carbon components (graphite or anthracite) were mixed with the determined content of resin P powder. This dry mixture was homogenized by mechanical stirring in a mortar at room temperature (RT). The composite samples consisted of 75 wt% carbon component (graphite or anthracite) and 25 wt% resin P.

Further samples were prepared by a second procedure (denoted Z), wherein resin P was used in the form of a solution; acetone was used as a solvent. The powdered carbon component (graphite or anthracite) was mixed with 25 wt% of dry resin in a solution (75% resin P solution in acetone) at RT, and this solution was homogenized with a magnetic stirrer (50 rpm) at RT for 2 h. The solvent was then evaporated at 100 °C in a vacuum chamber, and the obtained solid mixture was disintegrated using a mortar.

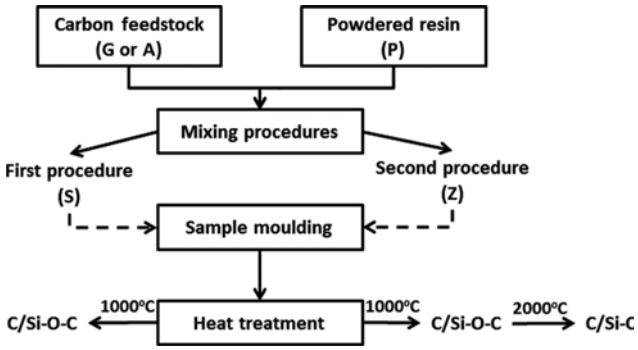

Fig. 1. Diagram showing the procedure of sample preparation.

The prepared powders from both procedures were then molded into cylindrical samples with a diameter of 12 mm. The compression molding was conducted at 110 °C under 16 MPa.

For clarity in the later text, the carbon/ceramic samples are denoted as follows:

- **GP-S**: samples prepared using graphite (G) and resin P according to the first procedure (S);
- **GP-Z**: samples prepared using graphite (G) and resin P according to the second procedure (Z);
- **AP-S**: samples prepared using anthracite (A) and resin P according to the first procedure (S);
- **AP-Z**: samples prepared using anthracite (A) and resin P according to the second procedure (Z).

To investigate the effect of the resin on the samples, reference samples were prepared with carbon components (graphite or anthracite) and the conventional CTP binder. CTP bonds to carbon grains when heated above its softening point (160 °C), and after carbonization, it becomes an efficient carbon binder.

Two separate heat treatment processes were carried out. In the first, the samples were heated in a one-step process to 1,000 °C, at a constant heating rate of 1 °C/min in an argon atmosphere, to manufacture C/Si-O-C composites (Fig. 1). In the second, samples were heated in a two-step process, initially to 1,000 °C at a constant heating rate of 1 °C/min, and subsequently to 2,000 °C at an average heating rate of 8 °C/min, both in an argon atmosphere, forming C/Si-C composites.

3. Apparatus and Methods

The total porosity of the samples was determined by hydrostatic weighing at RT. This parameter was calculated as the average taken from five measurements. The structure and phase composition of the composites after annealing to 1,000 °C and 2,000 °C were analyzed with the use of an X'Pert Pro (Philips) X-ray diffractometer (XRD) and an X-ray dispersive spectroscopy (EDS) extension coupled with scanning electron microscopy (SEM). The apparent crystallite size (height) was determined from the Scherrer formula (Eq. (1)):

$$L_c = K\lambda/(\beta \cdot \cos\theta) \quad (1)$$

where L_c is the crystallite height, K is the Scherrer constant (K= 0.9), λ is the wavelength of X-ray (λ=0.15418 Å), $\beta_{(hkl)}$ is the full width at half maximum (FWHM) of the (hkl) peak for graphite and SiC structures (in radians), and $\theta_{(hkl)}$ is the diffraction angle at maximum of the (hkl) band (in radians).

Microstructural observations were conducted with an optical microscope (OM, Carl Zeiss SteREO Discovery V8 microscope) and SEM (JEOL JMS-5400).

Oxidation resistance was determined by weighing the samples before and after isothermal oxidation at 600 °C for two hours in air,

thus determining the mass loss of samples as a result of oxidation. After cooling, the samples were weighed, and the percentage mass loss of the initial sample was calculated according to the following formula (2):

$$\%_{loss}=(m_i-m_f)/m_i\cdot 100\% \quad (2)$$

where: m_f is the final mass (g); and m_i is the initial mass (g).

Mechanical properties (compression strength, compression modulus) were determined on the Zwick testing machine model-1435 using a crosshead speed of 2 mm/min in laboratory conditions (RT), using cylindrical samples of C/Si-O-C and C/Si-C with dimensions of 5.5 mm length and 12 mm diameter. The mean values of compression strength, Young's (compression) modulus, and deformation at failure were determined on the basis of three individual measurements.

RESULTS AND DISCUSSION

1. Porosity Tests of Composite Samples

The total porosity values of the samples are listed in Table 3. The observed differences in the porosity indicate that the processing variables, i.e., compression molding temperature and pressure, as well as the initial carbon component (graphite or anthracite), have an impact on the total porosity of the samples.

Table 3. Porosity tests of samples obtained at 1,000 °C (C/Si-O-C) and 2,000 °C (C/Si-C)

Composites	C/Si-O-C	C/Si-C
	Total porosity, %	
Graphite/Coal tar pitch	30,5±2,1	
GP-Z	23,3±2,4	36,1±0,5
GP-S	34,8±1,9	41,1±0,7
Anthracite/Coal tar pitch	30,6±2,9	
AP-Z	29,9±3,9	41,3±1,0
AP-S	30,3±3,1	44,8±1,5

A characteristic feature of hot molded samples is the reduced compression pressure resulting from frictional resistance of the powder matrix, while maintaining a sufficiently high degree of compaction. This is most likely the effect of mutual movement of components and their susceptibility to uniform distribution. Lower sample porosity also resulted from the homogeneous distribution of the resin binder obtained during sample preparation. By using an organic solvent to modify the resin in the second procedure (Z), better carbon-polymer contact boundaries were created compared to the samples made according to the first procedure (S), i.e., without the solvent.

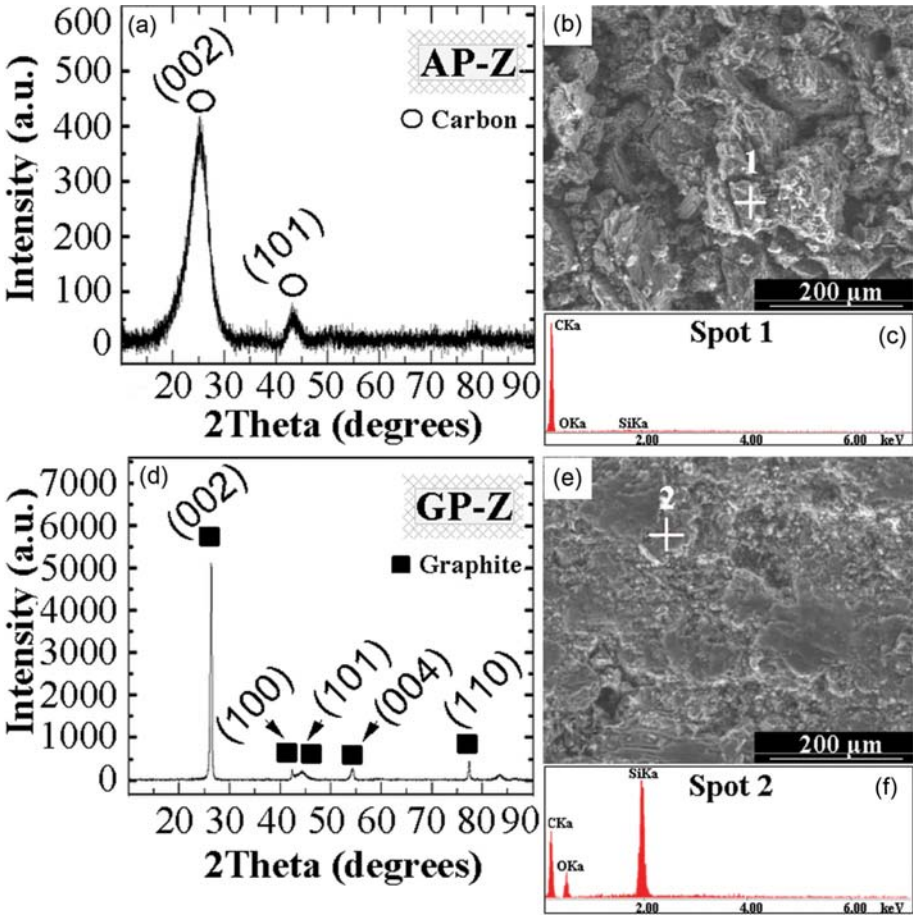

Fig. 2. SEM images, EDS, and XRD patterns of samples obtained with the use of graphite and anthracite after heating to 1,000 °C.

Higher porosity of the C/Si-C composites is mainly related to the formation of SiC during thermal decomposition of SiOC. During the heat treatment to 2,000 °C, hydrogen and sulfur-containing gaseous components are released, which causes an additional rise in the development of a porous matrix.

2. Microstructure and Phase Composition

Fig. 2 shows the SEM images, EDS, and XRD patterns of C/Si-O-C graphite- and anthracite-based samples after heat treatment to 1,000 °C. The micrographs (Fig. 2(b), (e)) indicate good compositional homogeneity after the molding step. The graphite-based samples (Fig. 2(e)) are particularly homogeneous; good adhesion with the polymer phase has been obtained. This demonstrates the suitability of the forming parameters, i.e., viscosity and temperature, of the impregnated samples in the initial phase of forming the composite samples. The samples contain pores of the order of 30-65 μm, which were generated after the thermal treatment process. This is particularly noticeable for anthracite-based samples (Fig. 2(b)), for which single pores merged to form larger pores.

The results of the EDS microanalyses confirmed the formation of Si-O-C after thermal treatment to 1,000 °C. Point analysis of the phase composition indicates the heterogeneity of the chemical composition. The different ratios of SiOC peaks are related to the effect of the carbon phase on the spectrum obtained, which is related to the intensity of the carbon derived peak (C).

The diffractograms show materials with various degrees of structural ordering, indicated by the intensity and shape of individual peaks. The low intensity and broad XRD peaks of the AP-Z sample, observed in Fig. 2, indicate low crystallinity in the structure of the carbon and ceramic components. In the case of graphite-based samples (GP-Z), the respective diffraction peaks are sharp and strong and do not change due to the temperature treatment.

The XRD patterns contain peaks at 2θ=22-26° and 43°. The first broad peak has been deconvoluted into two peaks which can be assigned to the carbon phase and the SiO_2 structure, probably in the form of a polymorphic tridymite. The peak identified at 2θ=43° corresponds to the graphite plane (100). A higher degree of structural ordering in graphite is also confirmed by the presence of peaks at 2θ=54-55° and 77°, which correspond to the (004) and (110) planes, respectively [23,24].

At the higher processing temperature (to 2,000 °C), the obtained samples show better structural ordering, indicated by sharper and stronger peaks at the angles of 2θ=24-26°, 43°, and 77.3°, as shown

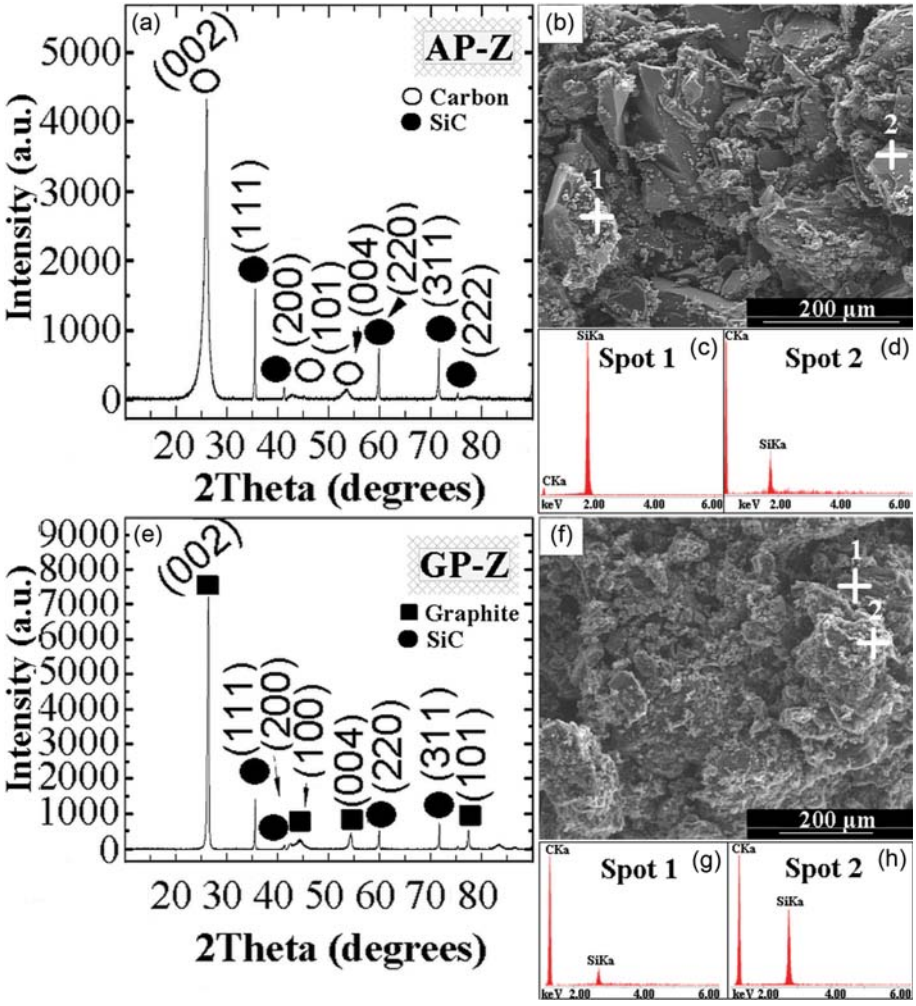

Fig. 3. SEM images, EDS and XRD patterns of samples obtained with the use of graphite and anthracite after heating to 2,000 °C.

Table 4. Diffraction peak values and basic parameters of carbon phases in C/Si-O-C and C/Si-C samples

Sample	C/SiOC			Sample	C/SiC		
	Reflection	$d_{(002)}$ [nm]	L_c (002) [nm]		Reflection	$d_{(002)}$ [nm]	L_c (002) [nm]
GP-Z	24,50	0,364	2,09	GP-Z	25,10	0,339	4,03
	26,21	0,337	14,09		26,40	0,337	13,84
AP-Z	23,53	0,356	2,40	AP-Z	24,30	0,342	4,23
	25,25	0,343	2,21		26,11	0,339	4,76

in Fig. 3. The intense diffraction peak at 2θ=26° of the samples obtained at 2,000 °C is related to carbon basal planes, (002). Additional peaks at the angles of 2θ=35-36°; 41-42°; 59-60°; 71-72°; and 75.5° are related to SiC crystallites with the structure of type 2H wurtzite and sphalerite 3C [24-27]. Thermal treatment to 2,000 °C leads to the conversion of the SiOC phase, forming SiC that is deposited on the surface of carbon grains and in the pores (Fig. 3(b), (f)). SiC occurs in the form of crystallites and cluster structures. The EDS analyses show that after annealing up to 2,000 °C, the oxygen peak disappears, resulting from the conversion of SiOC to SiC. Some basic parameters, determined from the identified characteristic peaks, are gathered in Table 4.

As a result of the thermal treatment of the composites, a product containing two carbon phases that differ in structural ordering is obtained. There are carbon components derived from the matrix and the so-called 'free carbon phase' formed by the thermal decomposition of the organic binder. The free carbon phase shows a partially ordered structure, which is a typical carbon phase known as a turbostratic carbon. It highlights the occurrence of the disordered phase, related to the absence of the ABAB sequence of graphene layers [28]. Based on the determined crystallite size, a better ordered carbon phase contains larger crystallites.

As is apparent from Table 4, increasing the temperature of treatment from 1,000 °C to 2,000 °C causes an increase in the size of crystallites of the carbon components. Another factor related to structural changes is the reduction of the interplanar distance, d_{002}. This indicates that the structural changes occurring in the carbon phase, originating from the conversion of resin to carbon residue, occurs through the rearrangement of basal graphite planes, leading to their better structural ordering (larger crystallites and lower d_{002} values).

The peaks at 2θ=24-26° and at 43-46° correspond to the two carbon phases: the base carbon component (graphite or anthracite) and the free carbon phase. In the case of graphite-based samples, small variations in crystallite size within the standard deviation occur. From this analysis, one may conclude that the crystallites in the graphite component are distinctly larger than those in the anthracite component; moreover, their size does not change due to heat treatment. Greater changes in the crystallite size and d_{002} interlayer spacings are observed for the anthracite-based samples.

The pyrolysis product obtained at 2,000 °C also contains the SiC ceramic phase that was derived from the resin precursor. Crystallite sizes of SiC, determined from XRD peaks for these samples, are listed in Table 5. The results show a small difference in SiC grain sizes between the samples. The AP-Z sample, containing anthracite, shows slightly larger SiC crystallites in comparison to the GP-Z sample, containing graphite.

Table 5. XRD data of silicon carbide

Sample	Crystallite size of SiC [nm]
GP-Z	24,2±2,8
AP-Z	26,2±2,2

Fig. 4 shows OM images of the surfaces of the C/Si-O-C and C/Si-C samples. The images enable qualitative information to be obtained on the microstructural distribution of the carbide phase binder.

The images show that the graphite grains are connected with continuous interphase boundaries (Fig. 4(a), (b), (d), (f)). The microstructure displays homogeneously deposited layers on the carbon grains, which may form a potential diffusion barrier against oxygen.

On the contrary, the anthracite-based C/Si-O-C samples show weak adherence of the SiOC binder (interphase boundary) to the surfaces of the carbon grains. It is likely that the resin was insufficiently distributed by the homogenization stage—where the resin and anthracite powder are mixed; thus the resulting ceramic residue (SiOC) does not fully cover the carbon grains (Fig. 4(c), (d), (g), (h)). Inappropriate distribution and weak resin penetration between the carbon grains result from their poor wettability by the resin. Poor spreading of the ceramic phase at the interface will cause a lower material stability at elevated temperatures under an oxidative atmosphere.

A significant increase in the ceramic coverage of anthracite grains was obtained after further heat treatment to 2,000 °C (Fig. 4(g), (h)). The probable mechanism of conversion from SiOC to SiC is the formation of silicon-containing gaseous compounds, which at higher temperatures decompose to form SiC. This allows for better penetration of the silicon-based compounds, via gas phase, into the porous microstructure of the sample, thus covering the carbon grains with SiC. Such a mechanism has been already described in one of our previous papers [29]. During thermal decomposition of pure polysiloxane resin (P) to 1,000 °C, SiO_yC_x-structures were obtained accompanied by formation of a turbostratic free carbon phase. Silicon-containing residues were identified by analyzing FTIR spectra of the samples obtained at different temperatures, from 1,000 °C up to 2,000 °C. The conversion mechanism of pure polysiloxane resin to SiOC and SiC carbide was shown. FTIR spectra of the ceramic residues obtained at 1,000 °C revealed a number of bands related mainly to the vibrations of the Si-O and Si-C, which indicated that the samples contained typical silicon oxycarbide compounds. During further heat-treatment above 1,700 °C, the spectra contained only the band derived from β-SiC. The struc-

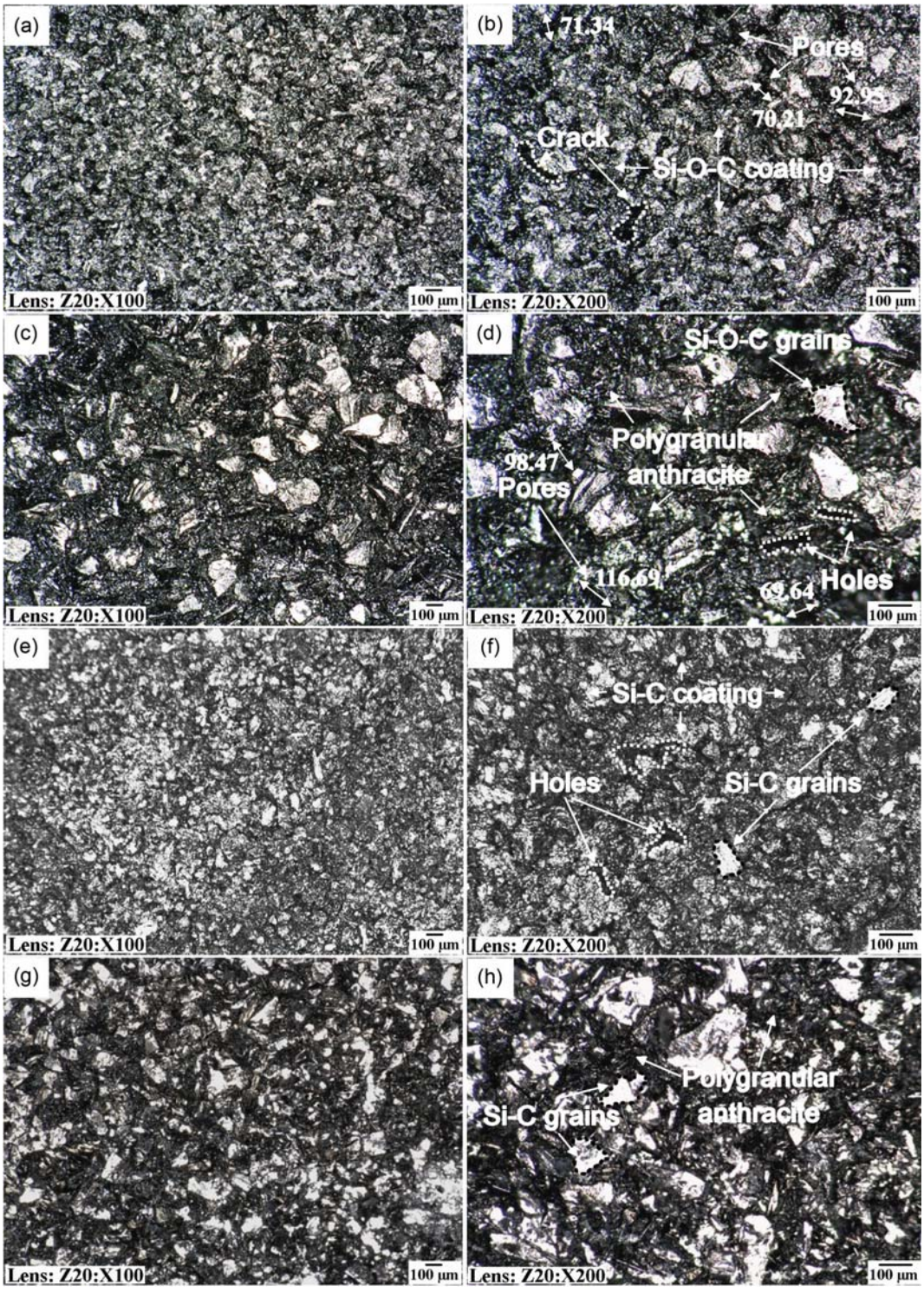

Fig. 4. Microstructure of samples: C/Si-O-C: (a), (b) GP-Z; (c), (d) AP-Z; and C/Si-C: (e), (f) GP-Z; (g), (h) AP-Z.

tural changes accompanying transforming silicone resin into silica ceramic residue have been the subject of research in works [30,31].

3. Isothermal Oxidation Test

The results of the C/Si-O-C and C/Si-C oxidation tests are presented in Figs. 5(a) and 5(b), respectively. The tests were conducted at 600 °C for two hours in air. Graphite- and anthracite-based samples manufactured with CTP binder were used as reference samples.

As predicted, these samples were completely oxidized after the tests. The lack of resin, which also acts as a ceramic precursor, means there is minimal oxidation resistance. The anthracite/CTP samples obtained at 1,000 °C show slightly lower (97.1%) mass losses compared to graphite/CTP samples (99.1%). This is due to a higher

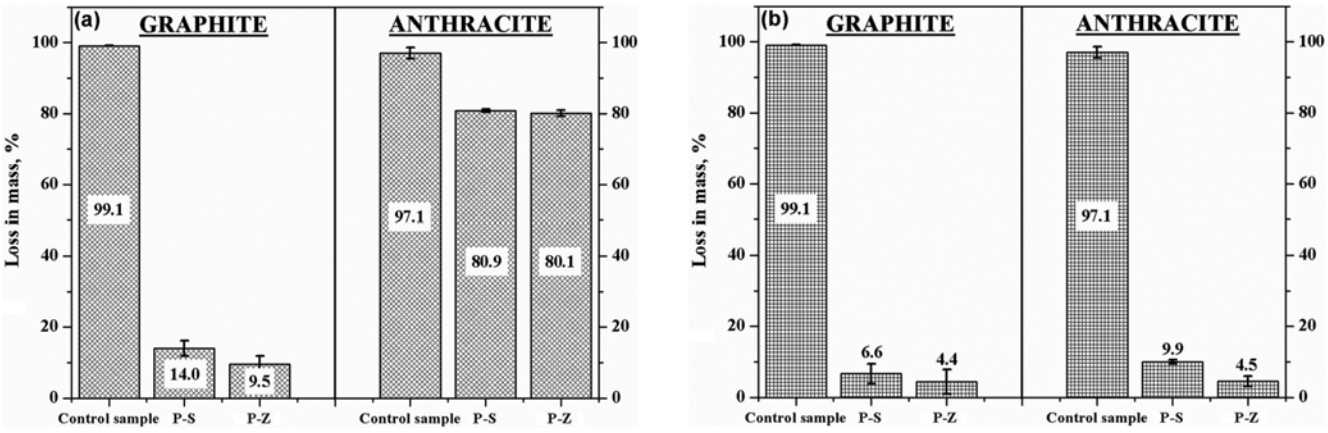

Fig. 5. Mass losses of (a) C/Si-O-C and (b) C/Si-C samples after the oxidation tests.

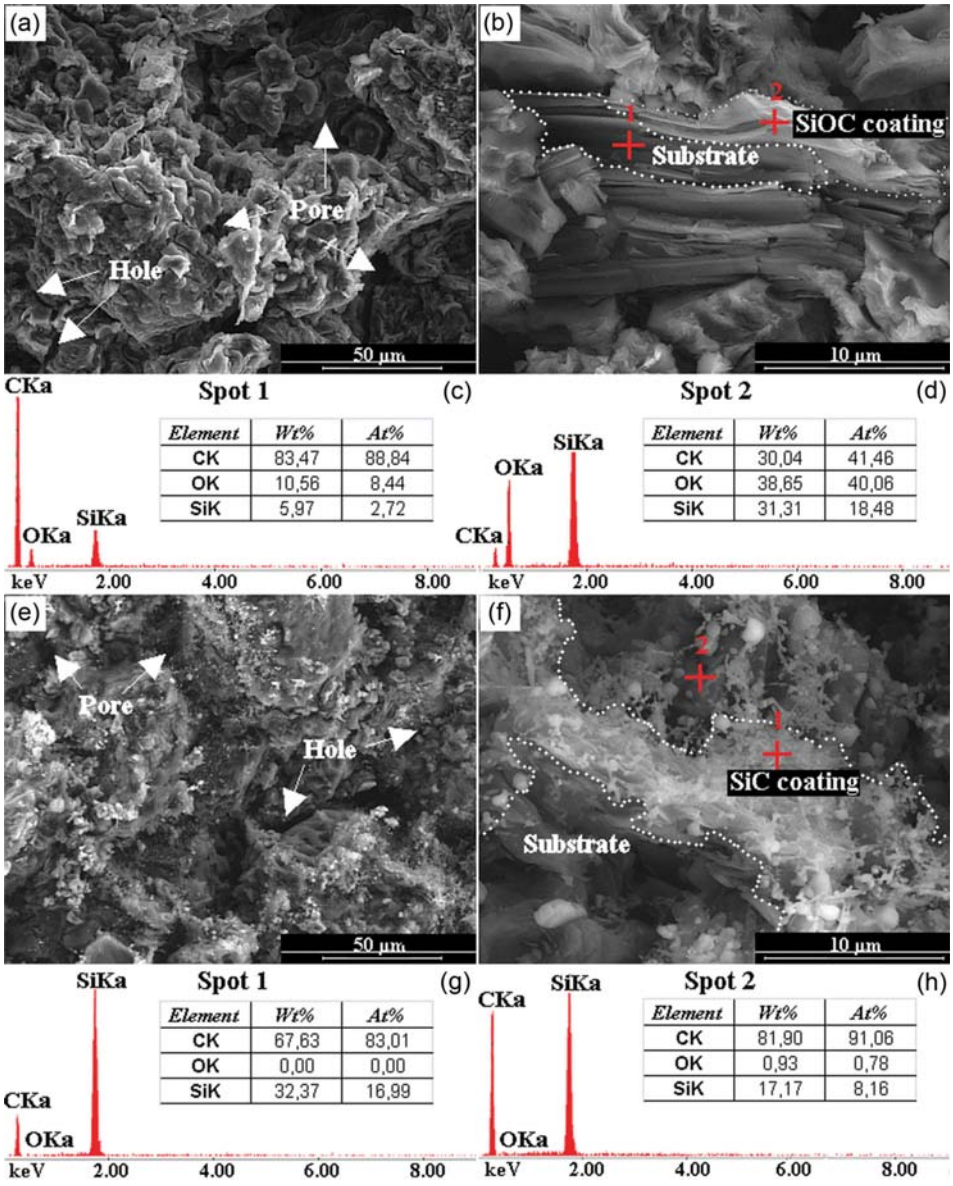

Fig. 6. SEM microphotograph of GP-Z composites: C/Si-O-C (a), (b); C/Si-C (e), (f) and ((c), (d), (g), (h)) EDS spectra at points 1, 2 indicated on the sample image.

concentration of metallic impurities in anthracite; these particles have a higher ash mass after oxidation.

In the case of resin-based graphite and anthracite samples, annealed to 1,000 °C, distinctly higher mass losses were noted for compositions with anthracite. While both samples contained ceramic binder in the form of SiOC (Fig. 5(a)), the microscopic observations of anthracite-based samples (Fig. 4) indicate that the grains are not coated with a continuous protective surface layer. A mass decrease in the anthracite-based samples was associated with higher oxidation exposure such that carbon surfaces were only partially coated with ceramic phase. On the contrary, a significant rise in oxidation resistance was observed for both samples after further heating to 2,000 °C, when the C/Si-C interphase boundaries were formed; no significant microstructural differences were seen after oxidation (Fig. 5(b)). This increased oxidation resistance is associated with the presence of a continuous ceramic layer on the carbon grains, their better adherence, and the higher resistivity of SiC to oxidation.

When analyzing the effect of the sample molding process, some differences can be observed between the samples formed by mixing dry components (first procedure, S) and those obtained using resin in solution (second procedure, Z). In general, samples obtained from the second molding process showed slightly lower mass losses, especially for graphite samples, which may be due to a more homogeneous distribution of the resin between the carbon grains. Uniform distribution of the resin phase creates a homogenous ceramic layer on the carbon grain surface, which forms a barrier to diffusion of the gaseous oxidant.

Fig. 6(a), (b) shows the cross-sectional morphology of the GP-Z sample impregnated with SiOC, and Fig. 6(e), (f)) the impregnated sample with SiC, after oxidation at 600 °C, for 2 hours.

As can be noted, oxidation of the sample leads to the creation of defects in the form of pores and cracks, visible on the microscopic images as dark areas. The C/Si-O-C sample (Fig. 6(a), (b)) is characterized by a porous carbon skeleton containing graphite grains covered with a continuous layer of SiOC as a result of appropriate wettability. EDS analysis (Fig. 6(c), (d)) showed that the presence of SiOC reduced the activity of the material to react with oxygen and reduced the formation of pores. A similar porous microstructure can be observed on GP-Z samples impregnated with SiC (Fig. 6(e), (f)); a uniform ceramic phase in the form of layers covering the graphite surface can be observed. A higher degree of material porosity (about 40%) is due to the gas phase SiC synthesis mechanism. Pores with a diameter of 30 μm are located mainly on graphite surfaces without SiC layers. According to the EDS analysis, a small amount of oxygen (0.93 wt%) was identified in the sample, which is likely to be the product of carbon oxidation.

Qualitative analysis of the oxidized composite samples was carried out using XRD; the diffractograms are shown in Fig. 7. The C/Si-O-C samples (Fig. 7(a)) demonstrate a distinct phase change after the oxidation tests, as compared to samples before oxidation (Figs. 2(a), (d) and 3(a), (d)). The observed difference is caused by the relatively high weight loss of anthracite-based sample (Fig. 5(a)) during oxidation, resulting from poor wetting of the anthracite grains by SiOC. Therefore, direct contact of the carbon phase with the oxidant causes its gradual degradation. This leads to an increase in

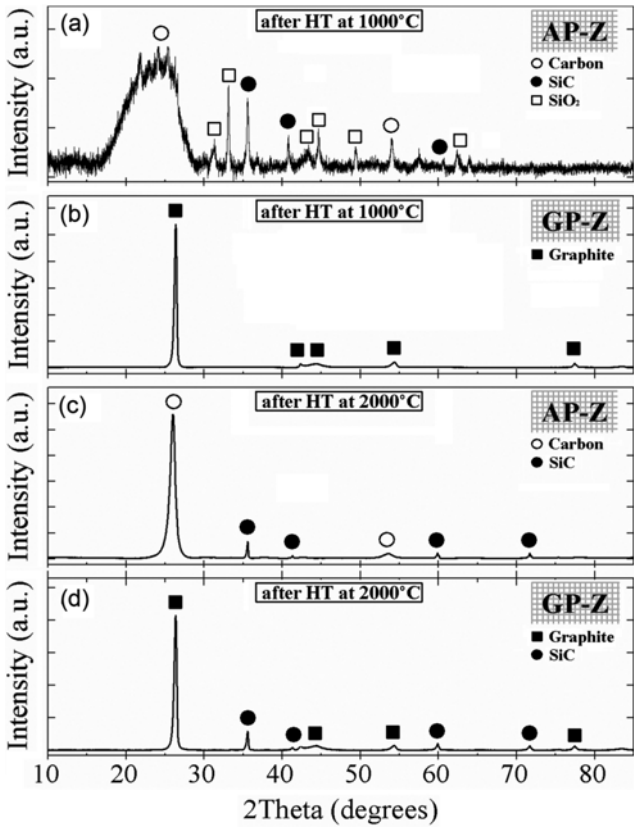

Fig. 7. XRD diffractograms of graphite and anthracite-based samples after the oxidation tests.

porosity and the formation of thermal stresses in the SiOC layer, which causes surface discontinuity (Fig. 6) [16].

As a result of SiOC phase oxidation, an amorphous silica glass is formed (Fig. 7(a)); the cristobalite structure can be observed in XRD patterns by the presence of peaks at 2θ=31-33°, as well as at 44.8°, 48.9°, and 53.5°. The following possible chemical reactions during oxidation can be proposed [23,32]:

In addition to the SiO_2 coating formed on the carbon surface (Eq. (5)), the oxidation reaction may lead to the release of (Si-O)- and ($C\text{-}O_x$)-containing gaseous compounds. The other XRD patterns (Fig. 7(b), (c), (d)) do not show any changes compared to those before oxidation. This is due to the protective coatings inhibiting oxidation.

$$C+O_2 \rightarrow CO_x \quad (3)$$

$$Si\text{-}C+O_2 \rightarrow Si\text{-}O\ (g)+CO\ (g) \quad (4)$$

$$Si\text{-}C+2O_2 \rightarrow SiO_2\ (s)+CO_x\ (g) \quad (5)$$

The kinetics of the oxidation process depends on the surface energy of the carbon phase, which is directly connected with structural and microstructural parameters (porosity, crystallinity), as well as with the purity of the material. The oxidation process, resulting from the favorable change of free energy, begins at about 400 °C. It takes place through the adsorption of oxygen from the atmosphere to active areas of the carbon material. Activation, due to favorable free energy changes, proceeds with simultaneous release of the heat

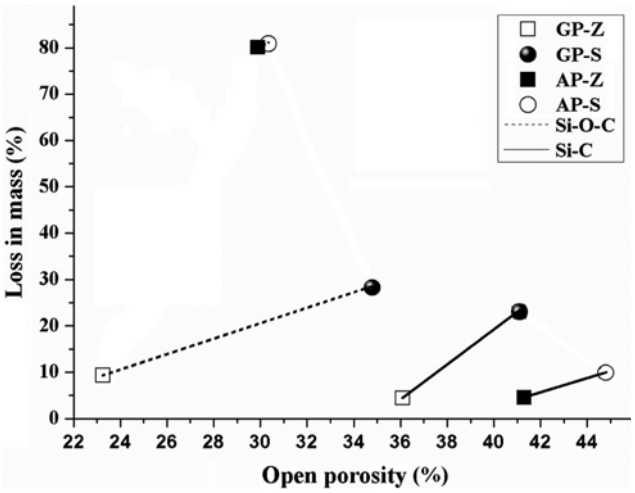

Fig. 8. Effect of samples porosity on oxidation resistance.

to the environment. The reaction between the active areas of carbon and oxygen, wherein carbon dioxide is formed, takes place more efficiently in porous or metal (Na, Fe) contaminated carbon materials. In the description of the oxidation kinetics, the material's structure should also be considered; the ideal crystal lattice (graphite), with a small presence of reactive disordered carbon, reduces the rate of reaction [1,4].

Note that the presence of the ceramic phase leads to a significant increase in thermal stability. The use of a ceramic binder with an inhibitor function interferes with the mechanisms that control the carbon-oxygen reaction, i.e., by blocking the active carbon sites and agents that act as catalysts at the oxidation temperature [5]. The reaction rate is decreased by filling active carbon areas with less active substances. Efficient thermal stability requires the use of a suitable ceramic modifier, uniformly distributed between carbon grains. Improved oxidation resistance was herein achieved by the conversion of silicon-containing resin to—depending on the annealing temperature—SiOC or SiC coatings on the carbon surface. Such coatings form a diffusion barrier to an oxidant.

The mass loss during the oxidation test as a function of porosity is shown in Fig. 8. Although C/Si-C composites show a higher volume of pores compared to C/Si-O-C composites, they are more resistant to oxidation. This is due to the specific properties of SiC, such as a low diffusion coefficient and high thermal durability, which makes this material one of the most favorable compounds for protection against oxidation [33], which is also confirmed by the obtained results.

4. Mechanical Properties

Values of the mechanical properties of carbon samples are presented in Table 6.

As shown in this table, the C/Si-O-C samples have significantly better mechanical strength than the C/Si-C samples. These favorable mechanical properties are a consequence of many different factors that determine the morphology and nature of the interphase boundary between the carbon grains. Based on the analysis of the composite sample components, carbon substrates are particularly important. The graphite grain component is less susceptible to deformation (shrinkage caused by mass loss) during thermal

Table 6. Mechanical properties of carbon-ceramic samples

Composites	Compression strength [MPa]		Young's modulus [GPa]	
	C/SiOC	C/SiC	C/SiOC	C/SiC
CTP	10,85±0,35		2,3±0,5	
GP-S	06,74±0,65	0,19±0,02	0,8±0,4	1,4±0,3
GP-Z	23,51±2,86	0,75±0,05	1,8±0,4	1,0±1,2
AP-S	04,20±0,86	0,11±0,01	2,0±0,1	1,2±0,1
AP-Z	04,65±0,65	0,23±0.02	1,4± 0.1	1,0±0,3

treatment; thus, better mechanical strength is obtained for the graphite-based composite samples than the anthracite-based samples. The interfacial strength, which influences the mechanical parameters of the composition, depends primarily on the physical and chemical matching of the components.

Impregnation of the carbon components with resin also affects the resulting mechanical properties. The results show that the strength of the composites obtained by mixing the components in solution (second procedure, Z) is higher. Unlike dry-blending (first procedure, S), this method facilitates phase homogenization, allowing for a uniform mixture to be obtained. Increasing the amount of carbon-resin contact leads to a more efficient distribution of the ceramic binder that is formed during the thermal treatment. A homogeneous arrangement of the binder ensures proper bonding to the carbon fraction, resulting in a material capable of bearing higher loads.

Graphite composite GP-Z demonstrates this further, where the C/Si-O-C compressive strength is over 70% higher than that obtained for GP-S. The anthracite-based C/Si-O-C composites also show this effect but to a lesser extent; the AP-Z composite has a compressive strength that is 10% higher than that of AP-S. Significant differences in the compressive strength were also observed for the C/Si-C samples. After high temperature treatment, both types of materials have significantly lower mechanical properties compared to the samples obtained at 1,000 °C. The graphite-based composites are characterized by distinctly higher strength compared to the anthracite-based composites. The influence of substrate type on the mechanical properties of the samples is related to their different behavior during thermal processing. The favorable behavior of the graphite-based composites is related to a lower amount of volatile compounds released during the thermal treatment as compared to the anthracite-based samples. This particularly applies to samples containing SiC, which are formed with a high gas phase influence.

From the point of view of mechanical parameters, it is particularly unfavorable to expose the composites to the oxidative treatment. As is evident from diagrams shown in Fig. 9, the mechanical properties are strongly correlated with the mass losses caused by the oxidation test.

All the samples significantly decrease their strength after oxidation. The behavior of the composites depends mainly on the type of binder used and its interaction with the carbon phase. The proper interaction between the wetting and subsequent carbon-binding components allowed for the formation of a stable material.

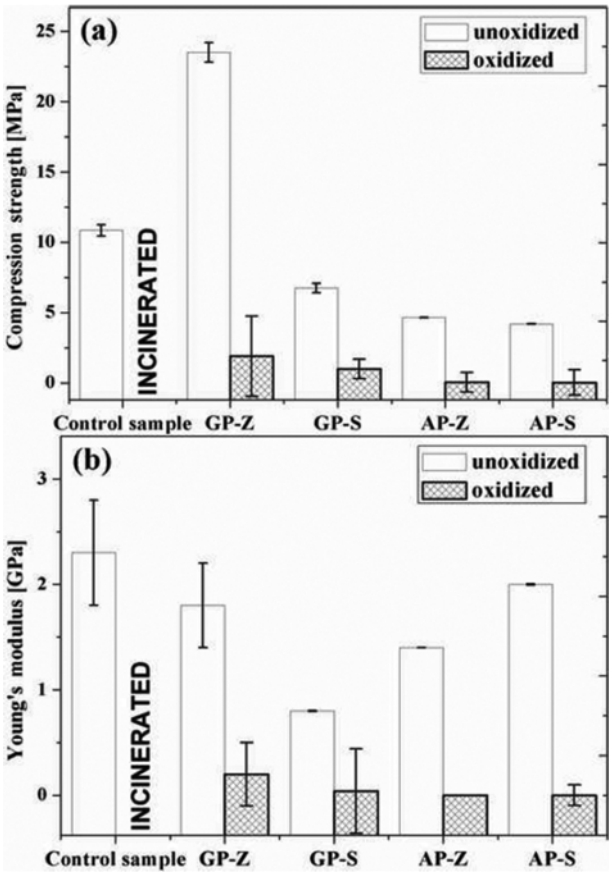

Fig. 9. Mechanical properties of carbon-silicon oxycarbide sample: (a) compression strength, (b) Young's modulus before and after oxidation test.

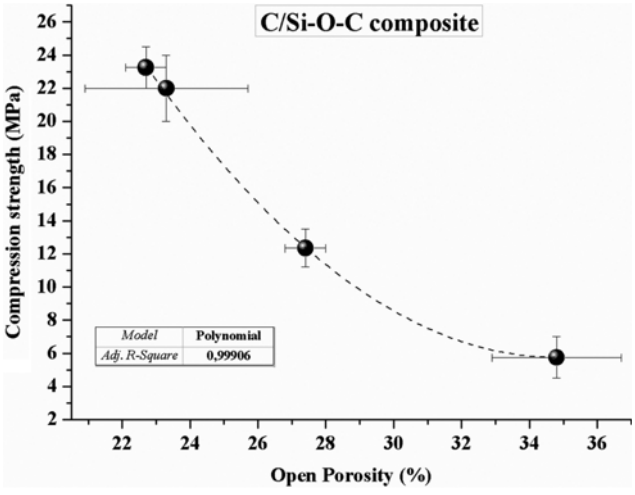

Fig. 10. Effect of porosity on compressive strength of graphite-based C/Si-O-C sample.

One of the most important factors affecting the mechanical parameters of the samples is their porosity. Fig. 10 shows changes in the compressive strength as a function of porosity. As is apparent from this figure, an increase in the material's porosity leads to a reduction in compression strength. The materials obtained are characterized by relatively high porosity. However, it can be expected that reducing the pore fraction—particularly the pores of large dimension by, for example, further liquid resin impregnation or recarbonization cycles, can improve oxidation resistance and mechanical properties.

CONCLUSION

Thermal treatment of carbon samples impregnated with polysiloxane resin allows porous carbon-ceramic composites to be obtained. Their thermal resistance under oxidation conditions depends on the applied material protection and its compatibility with the carbon structure. XRD analysis of the products obtained by heat treatment to 1,000 °C indicated the presence of two phases: carbon and oxycarbide (SiOC). The diffraction peaks related to those phases differed in intensity and shape, which resulted from various degrees of structural arrangement. Polysiloxane-derived ceramic residue obtained at 2,000 °C was confirmed to be SiC. The favorable properties of SiC, such as a low diffusion index and appropriate bonding with the carbon surface, make it possible to create a tight ceramic layer on the surface, which, despite relative high porosity of the materials, forms an effective diffusion barrier. Therefore, C/Si-C composites exhibit higher oxidation resistance. On the contrary, the mechanical properties of the composites are mainly related to porosity and the interaction between the two phases. The heat treatment to 1,000 °C, in which the thermal decomposition of polysiloxane resin forms SiOC, results in a less porous material than in the heat treatment to 2,000 °C. Hence the C/Si-O-C composites, which are less porous, show better mechanical properties.

ACKNOWLEDGEMENT

The work has been supported by the Polish National Centre for Research and Development, project no: PBS2/B5/27/2013 19.19.160.86540.

REFERENCES

1. D. W. McKee, *Fundamental Issues in Control of Carbon Gasification Reactivity*, **192**, 483 (1991).
2. L. M. Manocha, *Sadhana*, **28**, 349 (2003).
3. T. Sogabe, O. Okada, K. Kuroda and M. Inagaki, *Carbon*, **35**, 67 (1997).
4. G. Fitzer and L. M. Manocha, *Carbon Reinforcement and Carbon/Carbon Composites*, 281 (1998).
5. X. Wu and L. R. Radovic, *Carbon*, **44**, 141 (2006).
6. C. Isola, P. Appendino, F. Bosco, M. Ferraris and M. Salvo, *Carbon*, **36**, 1213 (1998).
7. W. Lu and D. D. L. Chung, *Carbon*, **40**, 1249 (2002).
8. S. Walter, G. D. Soraru, H. Brequel and S. Enzo, *J. Eur. Ceram. Soc.*, **22**, 2389 (2002).
9. G. D. Semchenko, I. Y. Shuteeva, O. N. Slepchenko and L. A. Angolenko, *Refractories and Industrial Ceramics*, **46**, 260 (2005).
10. W. Kowbel, J. C. Withers and P. O. Ransone, *Carbon*, **33**, 415 (1995).
11. C. T. Ho and D. D. L. Chung, *Carbon*, **28**, 815 (1990).
12. H. I. Yoo, H. S. Kim, B. G. Hong, I. C. Sihn, K. H. Lim, B. J. Lim

and S. Y. Moon, *J. Eur. Ceram. Soc.*, **36**, 1581 (2016).
13. T. L. Dhami, O. P. Bahl and B. R. Awasthy, *Carbon*, **33**, 479 (1995).
14. P. Lespade, N. Richet and P. Goursat, *Acta Astronaut.*, **60**, 858 (2007).
15. Y. C. Zhu, S. Ohtani, Y. Sato and N. Iwamoto, *Carbon*, **36**, 929 (1998).
16. L. M. Manocha, S. Manocha, K. B. Patel and P. Glogar, *Carbon*, **38**, 1481 (2000).
17. H. J. Li, H. Xue, Y. J. Wang, Q. G. Fu and D. J. Yao, *Surf. Coatings Technol.*, **201**, 9444 (2007).
18. C. Paluszkiewicz, T. Gumula, J. Podporska and M. Blazewicz, *J. Mol. Struct.*, **792**, 176 (2006).
19. K. Xia, C. Lu and Y. Yang, *New Carbon Materials*, **30**, 236 (2015).
20. M. Weinmann, E. Ionescu, R. Riedel and F. Aldinger, *Advanced Ceramics*, **2**, 1025 (2013).
21. M. A. Schiavon, E. Rodovanovic and I. V. P. Yoshida, *Powder Technol.*, **123**, 232 (2002).
22. F. Kolar, V. Machovic, J. Svitilova and L. Borecka, *Mater. Chem. Phys.*, **86**, 88 (2004).
23. O. S. Kwon, S. H. Hong and H. Kim, *J. Eur. Ceram. Soc.*, **23**, 3119 (2003).
24. M. A. Schiavon, S. U. A. Redondo, S. R. O. Pina and I. V. P. Yoshida, *J. Non. Cryst. Solids*, **304**, 92 (2002).
25. L. Duan, Q. Ma and Z. Chen, *J. Eur. Ceram. Soc.*, **33**, 841 (2013).
26. T. Gumula, C. Paluszkiewicz and M. Blazewicz, *J. Mol. Struct.*, **704**, 259 (2004).
27. T. Xu, Q. Ma, Y. Wang and Z. Chen, *Ceram. Int.*, **40**, 13787 (2014).
28. Z. Q. Li, C. J. Lu, Z. P. Xia, Y. Zhou and Z. Luo, *Carbon*, **45**, 1686 (2007).
29. T. Gumula, C. Paluszkiewicz and S. Blazewicz, *J. Anal. Appl. Pyrolysis.*, **86**, 375 (2009).
30. Q. Wu, Q. Zhang, L. Zhao, S. Li, L. Wu and J. Jiang, *J. Hazard. Mater.*, **336**, 222 (2017).
31. L. Guan, J. Gao, Y. Pei, L. Zhao, L. Gong, Y. Wan, H. Zhou, N. Zheng, X. Du, L. Wu, J. Jiang, H. Liu, L. Tang and Y. Mai, *Carbon*, **107**, 573 (2016).
32. X. Yang, Q. Huang, Z. Su, L. Chai, X. Wang and L. Zhou, *Ceram. Int.*, **39**, 5053 (2012).
33. M. Wang, L. Yang, C. Yu and C. Charles, *Ceram. Int.*, **38**, 2449 (2012).